

1 **Title Page**

2 **Manuscript title** The first description and quantitative assessment of the
3 conjunctival microcirculatory profile using a smartphone

4 **Author list (in order)**

5 1. Dr Paul F. Brennan^{1,2} 2. Dr Andrew J. McNeil³

6 3. Dr Min Jing⁴ 4. Miss Agnes Awuah¹

7 5. Professor Dewar D. Finlay⁴ 6. Professor Kevin Blighe¹

8 7. Professor James A.D McLaughlin⁴ 8. Professor Ruixuan Wang³

9 9. Professor Jonathan Moore¹ 10. Dr M. Andrew Nesbit¹

10 11. Professor EmanueleTrucco³ 12. Dr Mark S. Spence²

11 13. Professor Tara C.B. Moore¹

12 **Corresponding author** Professor Tara C.B. Moore¹

13 tara.mcmullen@ulster.ac.uk

14 **Institutions** ¹ *Biomedical Sciences Research Institute, Ulster University, Coleraine,*
15 *United Kingdom*

16 ² *Department of Cardiology, Royal Victoria Hospital, Belfast Health and Social Care*
17 *Trust, Belfast, United Kingdom*

18 ³ *VAMPIRE project, Computing (SSEN), University of Dundee, Dundee, United*
19 *Kingdom*

20 ⁴ *Nanotechnology and Integrated Bioengineering Centre (NIBEC), Ulster University,*
21 *Jordanstown, United Kingdom*

22 **Wordcount** 3324 words (excluding abstract, acknowledgements and references)

23 **Funding** This project was funded by Northern Ireland Chest Heart and Stroke
24 (NICHHS), the Ulster University and the Heart Trust fund, Royal Victoria Hospital,
25 Belfast, United Kingdom.

26 **Abstract**

27 **Purpose** The conjunctival microcirculation is a readily-accessible vascular bed
28 for quantitative haemodynamic assessment and has been studied previously using a
29 digital charge-coupled device (CCD). Smartphone video imaging of the conjunctiva,
30 and haemodynamic parameter quantification, represents a novel approach. We
31 report the feasibility of smartphone video acquisition and subsequent haemodynamic
32 measure quantification via semi-automated means.

33 **Methods** Using an Apple iPhone 6s and a Topcon SL-D4 slit-lamp
34 biomicroscope, we obtained videos of the conjunctival microcirculation in 4 fields of
35 view per patient, for 17 low cardiovascular risk patients. After image registration and
36 processing, we quantified the diameter, mean axial velocity, mean blood volume
37 flow, and wall shear rate for each vessel studied. Vessels were grouped into
38 quartiles based on their diameter i.e. group 1 ($<11\mu\text{m}$), 2 ($11\sim 16\mu\text{m}$), 3 ($16\sim 22\mu\text{m}$)
39 and 4 ($>22\mu\text{m}$).

40 **Results** From the 17 healthy controls (mean QRISK3 6.6%), we obtained
41 quantifiable haemodynamics from 623 vessel segments. The mean diameter of
42 microvessels, across all sites, was $18.23\mu\text{m}$ (range $6.6\sim 39.2\mu\text{m}$). Mean axial velocity
43 was 0.49mm/s (range $0.12\sim 0.79\text{mm/s}$) and there was a modestly positive correlation
44 ($r\ 0.404$) seen with increasing diameter, best appreciated when comparing group 4
45 to the remaining groups ($p<0.0001$). Blood volume flow (mean 109.718pl/s , range
46 $11.28\sim 502.19\text{pl/s}$) was strongly correlated with increasing diameter ($r\ 0.967$,
47 $p<0.0001$) and wall shear rate (mean 182.81s^{-1} , range $55.11\sim 546.69\text{s}^{-1}$) negatively
48 correlated with increasing diameter ($r\ -0.823$, $p<0.0001$).

49 **Conclusions** We, for the first time, report the successful assessment and
50 quantification of the conjunctival microcirculatory haemodynamics using a
51 smartphone-based system.

52

53 **Manuscript**

54 **I. Introduction**

55 Cardiovascular disease (CVD) is a leading cause, globally, of mortality and morbidity
56 while also being associated with a significant economic burden on health services¹.

57 CVD is caused by physiological changes and endothelial dysfunction, resulting in
58 atherosclerosis, and it is accepted that these changes manifest earliest in the

59 microcirculatory networks within the body². Microcirculatory disease typically

60 commences with endothelial dysfunction which may be clinically silent and, thus,

61 precede the onset of symptoms³ or the occurrence of a major adverse

62 cardiovascular event (MACE) e.g. myocardial infarction (MI) or cerebrovascular

63 accident (CVA). Microvascular dysfunction is associated with increased mortality⁴

64 and thus the study of microcirculations may provide a potential tool in disease

65 screening, staging and management. Imaging of systemic microcirculations has

66 been applied to and, in certain disease subsets, is used in every day current practice

67 in assessing disease progression e.g. the retinal microcirculation in the assessment

68 of diabetes mellitus, systemic hypertension, and sickle cell disease^{5,6,7,8}. The

69 sublingual mucosa and the skin also represent accessible sites in which the

70 microcirculation has been studied by videomicroscopy⁹.

71 The anterior segment of the eye contains the conjunctival microvasculature, a

72 readily-accessible heterogeneous network of arterioles and venules adjacent to the

73 limbal microcirculation, which gains its supply from the anterior ciliary branch of the

74 ophthalmic artery¹⁰. The conjunctival microvasculature allows for both non-invasive
75 assessment of erythrocyte movement, and quantification of key vascular
76 physiological parameters e.g. vessel width, blood flow axial velocity and blood flow
77 rate¹¹.

78 The objective of this study was to evaluate the feasibility of assessing the
79 conjunctival microcirculation using our novel combination of a smartphone and slit-
80 lamp biomicroscope. We aimed to develop an operator-friendly, pragmatic, safe and
81 effective means of assessing this heterogeneous circulation, in addition to the
82 quantification of the haemodynamic physiological parameters seen within a
83 microcirculation.

84 A few groups have reported semi-automated or automated image analysis
85 algorithms to assess the conjunctival microcirculation, using a slit lamp
86 biomicroscope and a digital charge-coupled device (CCD) camera for image
87 acquisition^{12,13,14,15,16,17}. Using such systems, the conjunctival microcirculation has
88 been studied in patients with hypertension, diabetic retinopathy, and patients after
89 ischaemic stroke^{18, 19, 20}. In addition, one group has reported the application of such
90 methods in patients of varying predictive cardiovascular risk, assessed by the
91 Framingham risk score²¹.

92 Smartphone technology allows for remote monitoring and screening of many
93 prevalent cardiovascular conditions, for example atrial fibrillation, and represents an
94 important component of future healthcare and cardiovascular practice²². The
95 literature is scarce regarding smartphone use to assess microcirculatory
96 haemodynamics but the application of smartphone photography of the fundus has
97 been reported in diabetic and hypertensive patients^{23, 24, 25}. [There are some studies](#)
98 [describing smartphone-led image analysis of the conjunctiva in the assessment of](#)

99 patients with anaemia^{26,27} and, also, quantification of conjunctival “redness” i.e.
100 hyperaemia²⁸. In addition, the smartphone-based biometric has been studied on the
101 visible vascular patterns on whites of the eye²⁹ but, at this time, there are no studies
102 that describe the assessment or quantification of conjunctival haemodynamics using
103 a smartphone and slit-lamp combination. ↓

Formatted: Font: Arial, Font color: Text 1, Pattern: Clear (White)

Formatted: Font: (Default) Arial, Font color: Text 1

Formatted: Font: (Default) Arial, Font color: Text 1

Deleted: Photography, using a smartphone, of the conjunctiva has been used in the assessment of anaemia²⁶ and quantification of conjunctival redness i.e. hyperaemia²⁷. There are no published reports of smartphone video imaging of the conjunctiva or assessment of the conjunctival haemodynamics.

Formatted: Font color: Text 1

105 **II. Materials and Methods**

106 **A. Subjects**

107 This research study was approved by the Research and Development review boards
108 of the Ulster University (UU) and the Belfast Health and Social Care Trust (BHSCT).

109 All subjects were provided with verbal and written information, prior to study
110 enrolment, in accordance with the Declaration of Helsinki. Exclusion criteria included
111 inability to consent, prior myocardial infarction (MI), uncontrolled systemic
112 hypertension, recent history of conjunctival inflammation, prior refractive surgery,
113 used ocular medications (other than artificial tears) and current use of contact
114 lenses.

115 We recruited 17 healthy volunteers to this feasibility study. The mean age for the
116 population studied was 52.5 ±10.3years, IQR 15 years. Sex distribution was roughly
117 equal with 9 (53%) males and 8 females (47%). No patients had a history of prior MI,
118 cerebrovascular accident (CVA), or diabetes mellitus. The well-validated QRISK 3

Formatted: Font color: Text 1

119 (<https://qrisk.org/three/>) score algorithm was used to estimate each volunteer's 10-
120 year risk of future heart attack or stroke. The QRISK 3 algorithm is based on the
121 presence/lack of specific risk factors for CVD e.g. smoking, diabetes mellitus,
122 hypertension, family history angina, chronic kidney disease, age, sex, body mass
123 index, history of atrial fibrillation, use of regular steroid tablets, presence of chronic

130 inflammatory disease, and cholesterol profile. The mean QRISK 3 score was 6.6
 131 $\pm 9\%$, IQR 6.9%, which correlates with a “low-risk” population (<10%)³⁰. Table 1 is a
 132 summary of the baseline demographics and clinical observations for the study group.

Commented [BP2]: Comments re. QRISK description addressed

Deleted: ²⁷

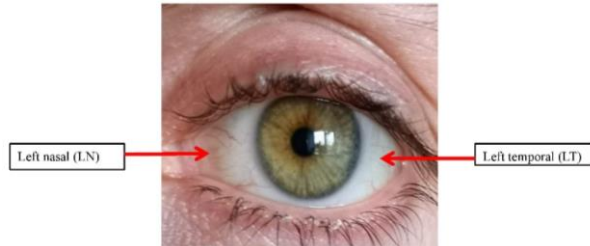
	Number n=17
<i>Male sex, n (%)</i>	9 (53.0)
<i>Age, years \pmSD</i>	52.5 \pm 10.3
<i>QRISK 3 score, % \pmSD</i>	6.6 \pm 9
<i>Systolic blood pressure, mmHg \pmSD</i>	125 \pm 22
<i>Diastolic blood pressure, mmHg \pmSD</i>	77 \pm 12
<i>Heart rate, bpm \pmSD</i>	70 \pm 9
<i>Prior MI/CVA/Diabetes mellitus</i>	0

133 Table 1. Baseline characteristics of the study group (n=17) with continuous variables
 134 expressed using their mean and standard deviation. Categorical variables have been
 135 expressed as a number and percentage of the total within that variable.

136 **B. Image Acquisition**

137 Image acquisition was achieved via two main hardware components. Firstly, primary
 138 illumination and magnification of the ocular vascular structure was achieved using a
 139 conventional slit lamp biomicroscope, Topcon SL-D4 (Topcon Medical Systems Inc.,
 140 USA), capable of providing a maximum magnification of 40x. Secondly, images
 141 provided by the slit lamp biomicroscope were further magnified and stored using a
 142 smartphone camera. The smartphone used in the system is an Apple iPhone 6s
 143 (Apple, Inc., USA). A number of video record settings were tested and the optimal
 144 configuration set at a resolution of 1920 x 1080 pixels, captured at 60 frames per
 145 second. The iPhone video recorder is capable of providing a further magnification of
 146 3x. Coupling of the smartphone to the eyepiece of the slit lamp biomicroscope was

148 achieved using a bespoke adapter developed by Zarf Enterprises (Zarf Enterprises.,
149 USA). Smartphone cameras typically give very little control over camera properties
150 (focus, ISO, shutter speed, aperture) due to an emphasis on ease-of-use for
151 everyday consumers, while also generating compressed video files (h.264
152 compression in the case of the iPhone 6s). To help overcome these issues we
153 captured our data using a third-party application "ProMovie Recorder"
154 (www.promovieapp.com). We used constant settings for all images (iso/shutter
155 speed/ focus/ exposure) and used the maximum compression bit-rate available to
156 reduce compression artefacts. The video zoom setting was locked at 2x, providing a
157 1:1-pixel mapping of the camera sensor at 1080p resolution and thus avoiding
158 interpolation artefacts. To obtain an accurate pixel to mm conversion factor we
159 calibrated the system using a digital caliper and 1mm microscope calibration reticle,
160 deriving a conversion factor of 552 ± 22.6 pixels/mm. We obtained one video (5-15s)
161 from 4 distinct field of views i.e. medial and temporal conjunctiva in both eyes. Fig.1.
162 To reduce eye motion and blinking we used an external fixation target as a focal
163 point for each patient. We acquired only 4 videos (5-15s) per patient to minimise the
164 risk of potential adverse effects, e.g. slit-lamp light exposure. There were no reported
165 adverse effects at the time of, or after, image acquisition. Patients were imaged in
166 the same clinical room under constant temperature and lighting settings.



167

168 Fig. 1. Two fields of view (FOV) for the left eye of a healthy subject, with the
169 medial and lateral FOV being labelled (red arrows) the left nasal (LN) and left
170 temporal (LT) respectively.

171

172

173 **C. Image Processing**

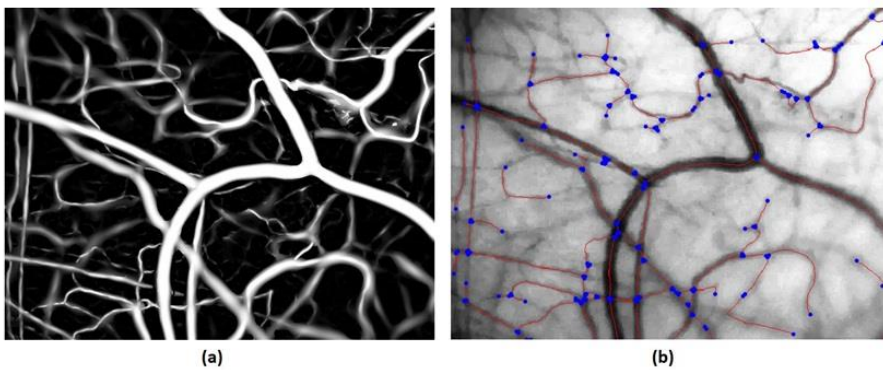
174 1. Pre-Processing and Vessel Segmentation

175 An initial pre-processing procedure was carried out for each video file. Firstly, the
176 longest stable sequence of frames was manually selected on the basis of the
177 vasculature being in focus, there being no blinking or large sudden movements of
178 the eye, and the FOV not drifting by more than ~25% of the width of the frame. Next
179 the green channel, which gave the highest vessel contrast, was extracted and
180 information from the red channel used to correct for uneven illumination through
181 subtraction. The sharpest frame in the sequence was then selected as a reference
182 frame and all other frames registered to it through an affine registration procedure³¹
183 with a single composite image generated by averaging all registered frames. After
184 applying a “vessel enhancement filter”³² (Fig.2 (a)), a binary map of the conjunctival

Deleted: 29

Deleted: 0

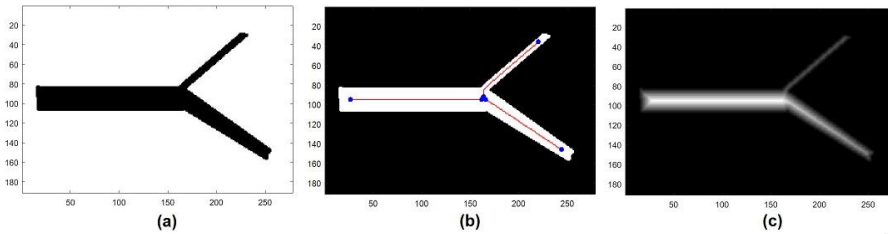
187 vasculature and corresponding centrelines were obtained via standard skeletisation
188 techniques. Finally, the connected vessel network was broken into individual vessel
189 segments (Fig.2 (b)) by setting the branch points' neighbouring pixels to zero, and
190 centreline segments, containing more than 30 pixels, selected for further
191 assessment.



192 (a) (b)
193 Fig. 2. Microvascular network after image processing: (a) the vessel network after
194 filtering; (b) the vessel centreline (in red) and intersection points (in blue) overlaid on
195 the mean of vessel images.

196 2. Vessel Diameter (D)

197 The Euclidean Distance Transform (EDT) was proposed for vessel diameter
198 estimation, which is easier to implement in comparison to the commonly used
199 method via full width at half maximum (FWHM). The value at each pixel of EDT was
200 calculated based on the Euclidean distance between the pixel and its nearest
201 nonzero pixel in the binary vessel image. The centreline of the vessel was used to
202 obtain the central EDT values and thus the radius along the vessel axis. The
203 average of diameters along the vessel length provided the final vessel width
204 estimation. An example based on simulation is illustrated in Fig.3.



205

206 Fig. 3. Simulation for vessel diameter estimation: (a) three vessels are generated
 207 with mean diameter 25.3 pixels, 16.5 pixels, and 8.3 pixels, respectively; (b) the
 208 vessel centrelines, end points and branch points overlaid on the binary vessel
 209 image; (c) EDT of the binary vessel image. The mean of estimated diameters via
 210 EDT are 25.9 pixels, 16.6 pixels, and 8.6 pixels, respectively.

211 Given the complex and heterogeneous distribution of conjunctival microvessels, we
 212 applied a grouping classification to our results, described in previous work, based on
 213 vessel D i.e. group 1 ($<11\mu\text{m}$), group 2 ($11\text{-}16\mu\text{m}$), group 3 ($16\text{-}22\mu\text{m}$) and group 4
 214 ($>22\mu\text{m}$)¹¹.

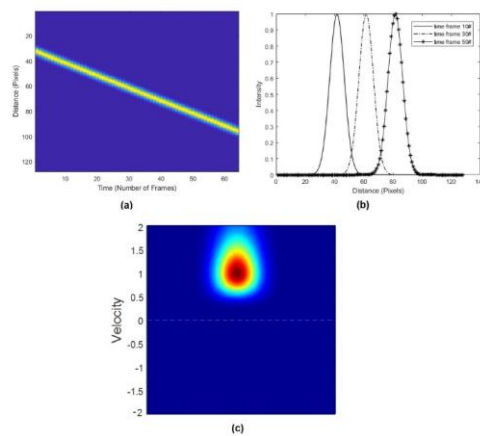
215 3. Axial velocity (V_a)

216 The blood flow V_a in a single vessel segment was estimated based on the spatial-
 217 temporal image (STI), with the change in intensity in STI reflecting erythrocyte
 218 movement through the vessel. Since STI signal is the one dimension of space plus
 219 time, i.e., a 1D+T signal, a novel approach based on spatial temporal 1D+T
 220 continuous wavelet transform (1DTCWT) is proposed for V_a estimation. The CWT
 221 method has been used previously as a spatiotemporal filter for motion capture of
 222 1D+T signals for moving target tracking and parameter calculation³³, but not yet
 223 exploited in microvascular blood flow velocity estimation. Firstly, 2D fast Fourier
 224 transform (FFT) is performed for STI. The velocity vector space is defined and

Deleted: 1

226 1DTCWT is then run at each time interval. The energy is subsequently calculated
227 based on the 1DTCWT output. The velocity is obtained by searching the maximum
228 energy point as shown in Fig.4. The average of the absolute velocity across all
229 frames was used as the final estimation of V_a . The method was programmed in
230 MATLAB2017 together with an open source implementation of CWT ³⁴

Deleted: ²



231

232 Fig.4. Simulation for velocity estimation based on 1DTCWT. (a) synthetic STI
233 generated by shifting Gaussian signal with speed of 1 pixel/frame; (2) plot of
234 signals at the 10th, 30th and 50th frames, which shows the Gaussian signal
235 shifting in distance; (c) a colour spectrum map via 1DTCWT shows the velocity is
236 corresponding to the maximum of the energy (at 1 pixel/frame).

237 4. Blood flow (Q) and wall shear rate (WSR)

238 Using the measurements for D and V_a , we calculated Q and WSR using previously
239 described methods ^{11,12}. Q provides key information regarding the architecture and
240 function of the vascular system, whereas WSR is the blood velocity at a specific wall

242 position, within a vessel, and represents a surrogate for the pressure exerted by
243 blood within its' respective transport vessel ^{35, 36, 37}

Deleted: 3

Deleted: 4

Deleted: 5

244

245 5. Statistical analysis

246 For statistical analysis SPSS for Apple iOS version 25 (property of IBM) and R
247 version 3.5.3 (www.r-project.org) were used. Continuous variables were described
248 using the mean, standard deviation of the mean and interquartile range (IQR) for the
249 variable. Categorical variables were described as a number and percentage of the
250 total category number to which the variable belonged. Sample origin, distribution and
251 variance were assessed by non-parametric ANOVA (Kruskal-Wallis test). Correlation
252 analysis (Spearman rank), with a Loess regression fit, was applied to assess
253 relationships between D and independent variables, principally Va, Q and WSR.
254 Non-parametric ANOVA (Kruskal-Wallis) with or without Dunn's post-hoc tests was
255 used to compare D, Va, W, and WSR by vessel width group, with the tests being
256 conducted separately across site, i.e., left/right nasal and temporal, or for all sites
257 merged.

258 III. Results

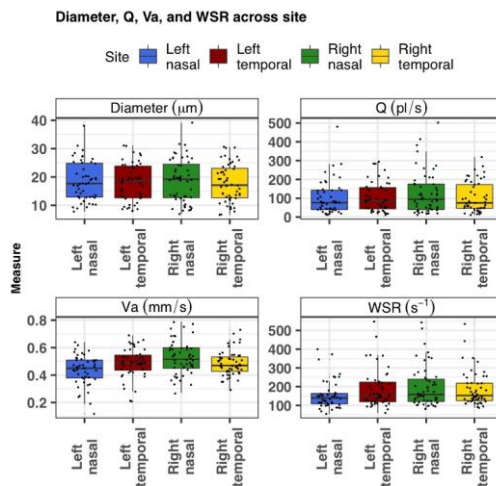
259 For the 17 healthy patients studied, using our semi-automated approach, we were
260 able to obtain repeated measurements in 623 vessel segments (mean 37 segments
261 per patient), hereafter referred to as "microvessels", which exhibited observable flow.
262 The mean diameter (D) of microvessels, across all sites, was 18.2 μ m (range 6.6-
263 39.2 μ m). Group 4 (>22 μ m) microvessels were measured most frequently, with group
264 1 (<11 μ m) being the least commonly encountered i.e. 295 vs 64 microvessels
265 respectively. Mean Va was 0.49mm/s (range 0.12-0.79mm/s), Q 109.72pl/s (range

269 11.28-502.19pl/s) and WSR ranged between 55.11-546.69s⁻¹, with a mean WSR of
 270 182.81s⁻¹. The mean and SD of all microvessel conjunctival haemodynamic
 271 parameters are illustrated in Table 2. Statistical comparisons for Va, Q and WSR
 272 were made within the vessel groups. There was a statistically significant increase in
 273 Q for increasing diameter size (p<0.0001), with a statistically significant inverse
 274 correlation between WSR and increasing diameter size (p<0.0001). Va tended to
 275 increase with increasing microvessel diameter and was significantly elevated in
 276 group 4 (>22µm) vessels, compared to the remaining three groups (p<0.0001).
 277
 278

Group D µm	No. vessels N=623	D (µm)	Va (mm/s)	Q (pl/s)	WSR (s⁻¹)
<11 Group 1	64	9.1 ±2.8	0.45 ±0.05	23.65 ±2.96	332.75 ±60.75
11~16 Group 2	113	13.44±3.7	0.44 ±0.06	46.81 ±8.02	200.19 ±32.89
16~22 Group 3	151	19.2 ±3.5	0.47 ±0.06	97.13 ±17.21	136.67 ±20.35
>22 Group 4	295	26.9 ±2.7	0.56 ±0.09	224.45 ±66.35	115.27 ±17.7
			p<0.0001	p<0.0001	p<0.0001
	Mean	18.2	0.485	109.718	182.81
	Range	6.6-39.2	0.12-0.79	11.28-502.19	55.11-546.69
	Interquartile range (IQR)	12.74-24	0.42-0.55	39.86-161	116.33- 221.72

279 Table 2. Summary of haemodynamic measures D, Va, Q and WSR based on the
280 vessel diameter groups (1-4).

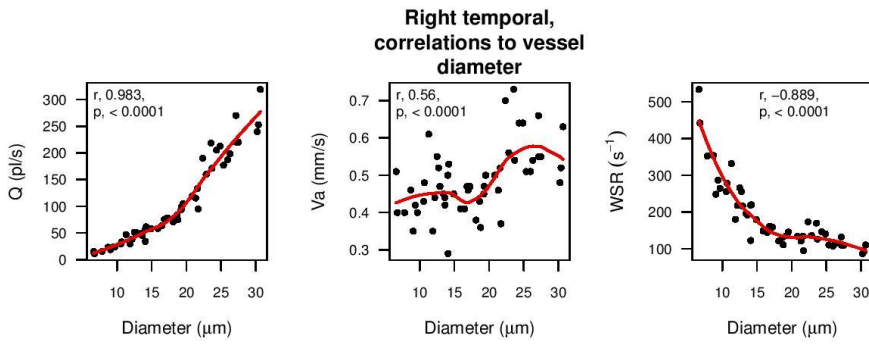
281 Across site (field of view) comparisons were made with the haemodynamic
282 measures. Q and WSR did not statistically differ between the 4 image fields. There
283 was a statistically higher Va noted in the right nasal (RN) hemisphere compared to
284 the left nasal (LN, ($p = 0.0003$)), for which the clinical significance is unknown and
285 may require further exploration. The relationship between the haemodynamic
286 measures and similarities for each field of view is shown in Fig.5. Note the elevated
287 Va in the RN FOV, compared to the other FOVs, as before.



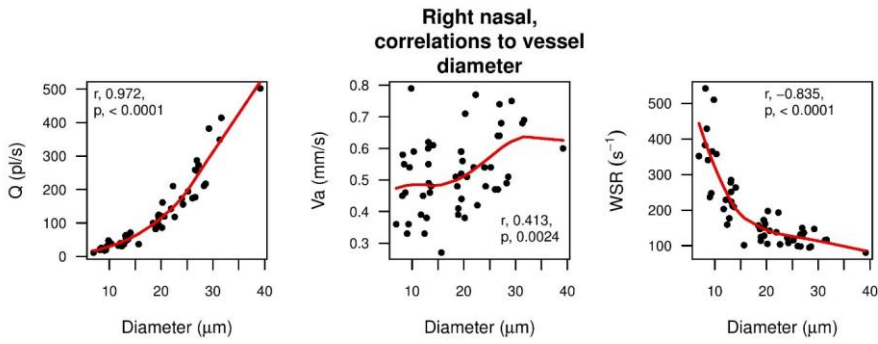
288
289
290 Fig.5. Summary of diameter D (μm), Va (mm/s), Q (pl/s) and WSR (s^{-1}), for each field
291 of view i.e. left nasal (LN), left temporal (LT), right nasal (RN) and right temporal
292 (RT).

293 The correlation, expressed via the correlation coefficient (r) and the best fit trend line,
294 between increasing microvessel diameter and the haemodynamic measures Va, Q
295 and WSR were consistent across the 4 fields of view, which are individually

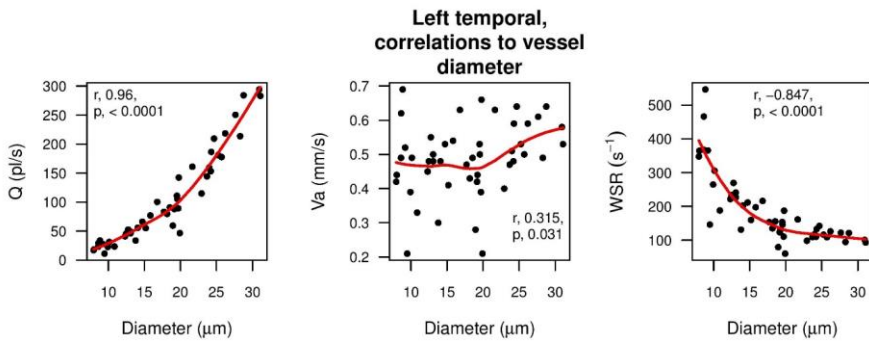
296 illustrated in Fig.6a-d.



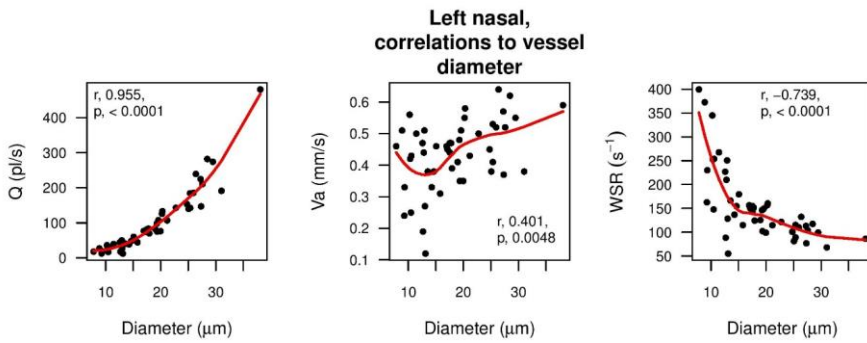
297



298

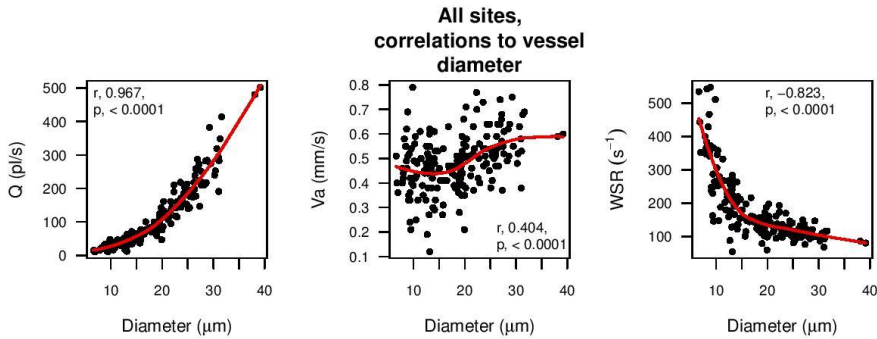


299



300
 301 Fig.6. Correlation plots between microvessel diameter D (μm) vs V_a (mm/s), Q (pl/s)
 302 and WSR (s^{-1}) for each field of view ((a) RT, (b) RN, (c) LT, (d)LN).

303 A summary of the correlations between microvessel D and the quantified
 304 haemodynamic measures are illustrated in Fig.7. demonstrating the strong overall
 305 linear correlation with Q and WSR (r 0.967, r -0.823 respectively). A modest
 306 correlation was seen for V_a (r 0.404).



307
 308 Fig.7. Correlation plots between microvessel diameter D (μm) vs V_a (mm/s), Q (pl/s)
 309 and WSR (s^{-1}) across all sites.

310 The correlations between increasing vessel diameter and V_a , Q , and WSR are in
 311 keeping with that reported in previous work^{11,12}, whereby similar fluid dynamics and
 312 microvascular relationships have been observed.

313

314

315 **IV. Discussion**

316 The conjunctival microcirculation represents a readily-accessible vascular network
317 for non-invasive assessment. Physiological measures in the conjunctival
318 microcirculation display the same trends and correlations as they do elsewhere in
319 the circulation and, based on this rationale, may represent a key microcirculation that
320 could be assessed in the evaluation of circulatory health and, if so, correlated with
321 risk. Correlations between cardiovascular risk estimation and quantitative
322 conjunctival haemodynamic measures, namely velocity and blood flow, were
323 demonstrated in previous work²¹.

324 In recent years, there have been several reports regarding the clinical utility of
325 conjunctival microcirculatory study. Conjunctival haemodynamic assessment has
326 extended to patients with diabetes mellitus, in correlation with diabetic retinopathy
327 status, with differences between Va, Q and WSR being observed for differing grades
328 of retinopathy¹⁹. Quantitative assessment of the conjunctival haemodynamics was,
329 also, evaluated in patients with ischaemic unilateral stroke and Va was found to be
330 significantly lower in the ipsilateral eye to the stroke compared to the contralateral
331 eye, demonstrating the physiological relationship shared by the internal carotid
332 arterial system and the conjunctival microcirculation²⁰.

333 We have described the application of smartphone technology, combined with a slit-
334 lamp, in the quantitative assessment of conjunctival haemodynamics, namely D, Va,
335 Q and WSR. With our approach, we have demonstrated the feasibility of obtaining
336 haemodynamic results, similar to the correlations and trends described elsewhere by
337 other groups using a digital charged coupled camera. We have done so, though,
338 using a smartphone which served as an efficient, pragmatic and reliable means of

Formatted: Font color: Text 1

339 acquiring the conjunctival images for subsequent analysis. Our system performed as
340 well as the more complex and time-consuming CCD devices and represents a
341 potential major advancement within the scope of conjunctival microcirculation
342 assessment. Our biomicroscope/smartphone apparatus and post-capture analysis is
343 validated by comparison to results obtained previously. We obtained a mean
344 diameter of 18.2µm (range 6.6-39.2µm) in 623 microvessels, selected manually
345 according to the quality of STI, on post-processed images and these results are
346 similar to, and within range, of that reported by other groups¹¹. The strong
347 positive/negative correlation between microvessel diameter (D) and blood flow (Q)/
348 wall shear rate (WSR), reported in the present work, is in keeping with that found in
349 other studies^{11, 12,13}. We did not find as strong a correlation for axial velocity (Va) and
350 diameter (D) ($r = 0.404$), compared to that observed for blood flow (Q) and wall shear
351 rate (WSR). Statistical significance, though, was observed for group-4 vessels and
352 their associated Va, compared to groups 1-3 ($p < 0.0001$).

353 Combined smartphone and slit-lamp based quantitative assessment has been
354 demonstrated in this present work and it is feasible that it could be of potential future
355 application, in the assessment of cardiovascular health. We studied a “low-
356 cardiovascular risk” patient group, as evidenced by a mean QRISK 3 score of 6.6%.
357 QRISK 3 is a well-validated 10-year cardiovascular risk assessment, with the largest
358 sample size of contemporary cardiovascular estimation systems, implemented within
359 major European guidelines³⁰,

360 We acknowledge certain limitations of our study. We, similar to other feasibility
361 studies¹³, have reported results for all visible microvessels without separating
362 arterioles and venules. The feasibility of artery-vein classification, using our
363 approach, in the conjunctiva requires further exploration, which we intend to pursue.

Deleted: Combined smartphone and slit-lamp-based quantitative assessment has been demonstrated in this present work...

Formatted: Font color: Text 1

Deleted:

Deleted: ied

Deleted: ²⁷

370 In addition, cardiac-gated haemodynamic measures, primarily end-systolic and end-
371 diastolic measures using conjunctival vessel pulse waveform characteristics, have
372 been reported previously and could be of potential use in future clinical application
373 with certain cardiovascular disease subsets³⁵. A key aim of our future work is to
374 implement and validate a fully automated smartphone-based approach to remove
375 potential human error, promote consistency, and improve the efficiency of the
376 examination. By quantifying the conjunctival haemodynamics our method potentially
377 allows the inexpensive assessment of patients with established cardiovascular and
378 systemic disease, with promise for improving the diagnosis, risk stratification and,
379 potentially, evaluating disease status and treatment modification of cardiovascular
380 disease(s). The addition of smartphone technology, with its APP versatility, wealth of
381 data management, and computerised machine learning algorithms, to a slit-lamp
382 biomicroscope potentially modernises the assessment of the conjunctival
383 microcirculation.

Deleted: 2

384 V. Conclusion

385
386 We have described, for the first time, the successful measurement of dynamic
387 microcirculatory haemodynamic measures using smartphone technology combined
388 with a slit-lamp biomicroscope. Our semi-automated method found a positive linear
389 relationship between increasing microvessel diameter (D) and blood flow (Q). An
390 inverse relationship was observed for wall shear rate WSR, a direct surrogate of
391 WSS. These findings corroborate prior ones, for the same haemodynamic measures,
392 reported by groups using a CCD camera for image acquisition, and support the
393 feasibility of our smartphone-derived approach. Image acquisition was performed
394 without clinical complication in a group of patients with low cardiovascular risk. The

Deleted:

Deleted: Further hardware and software development is required to assess if a "smartphone-only" approach, without the need for a slit-lamp, can be used to reliably quantify the conjunctival haemodynamics.

Formatted: Font color: Text 1

401 ease and speed with which images were reliably acquired holds promise for the
402 future clinical application of this smartphone-based conjunctival microcirculatory
403 assessment model.

404

405

406 **VI. Acknowledgements**

407 This project was funded by Northern Ireland Chest Heart and Stroke (NICHHS), the
408 Ulster University and the Heart Trust fund, Royal Victoria Hospital, Belfast, United
409 Kingdom.

410 **VII. Disclosure/Conflict of interests**

411 The authors, collectively, have no conflicts of interest or anything to disclose with
412 respect to this original research manuscript.

413

414 **VIII. Reference list**

- 415 1. Bhatnagar P, Wickramasinghe K, Williams J, et al. The epidemiology of
416 cardiovascular disease in the UK 2014. *Heart*. 2015; 101:1182-1189
- 417 2. Stokes KY, and Granger DN. The microcirculation: a motor for the
418 systemic inflammatory response and large vessel disease induced by
419 hypercholesterolaemia? *J. Physiol*. 2005; 562:647-653
- 420 3. Krentz AJ, Clough G, Byrne CD. Vascular disease in the metabolic
421 syndrome: Do we need to target the microcirculation to treat large
422 vessel disease? *J Vasc Res*. 2009; 46:515-526
- 423 4. Liew G, Mitchell P, Rochtchina E, Wong TY, Hsu W, Lee ML, Wainwrig
424 ht A, Wang JJ. Fractal analysis of retinal microvasculature and
425 coronary heart disease mortality. *Eur Heart J*. 2011; 32: 422-429

- 426 5. Cheung et al. Correlation of microvascular abnormalities and
427 endothelial dysfunction in type-1 diabetes mellitus (T1DM): A realtime
428 intravital microscopy study, *Clin. Hemorheol. Microcirc.* 2009; 42(4):
429 285–295
- 430 6. Wong TY, Klein R, Sharrett AR, Duncan BB, Couper DJ, Tielsch JM,
431 Klein BE, Hubbard LD. Retinal arteriolar narrowing and risk of coronary
432 heart disease in men and women. The Atherosclerosis Risk in
433 Communities Study. *JAMA.* 2002; 287:1153–1159
- 434 7. Wanek J, Gaynes B, Lim JI, Molokie R, Shahidi M. Human bulbar
435 conjunctival hemodynamics in haemoglobin SS and SC disease. *Am.*
436 *J. Hematol.* 2013; 88(8): 661–664
- 437 8. Cheung et al. Microvascular abnormalities in sickle cell disease: A
438 computer-assisted intravital microscopy study. *Blood.* 2002;
439 99(11):3999–4005
- 440 9. Houben AJHM, Martens RJH, Stehouwer CDA. Assessing
441 microvascular function in humans from a chronic disease perspective.
442 *JASN.* 2017; 28(12):3461-3472
- 443 10. Van Buskirk EM. The anatomy of the limbus. *Eye (Lond).* 1989;
444 3(2):101-8.
- 445 11. Khansari MM, Wanek J, Felder AE, Camardo N, Shahidi M. Automated
446 assessment of hemodynamics in the conjunctival microvasculature
447 network. *IEEE Transactions on Medical Imaging.* 2016; 35:605-611
- 448 12. Koutsiaris et al. Volume flow and wall shear stress quantification in the
449 human conjunctival capillaries and post-capillary venules in vivo.
450 *Biorheology.* 2007; 44(5): 375–386

- 451 13. Shahidi M, Wanek J, Gaynes B, Wu T. Quantitative assessment of
452 conjunctival microvascular circulation of the human eye. *Microvasc*
453 *Res.* 2010; 79(2):109-13
- 454 14. Koutsiaris AG, Tachmitzi SV, Papavasileiou P, Batis N, Kotoula MG,
455 Giannoukas AD, Tsironi E. Blood velocity pulse quantification in the
456 human conjunctival pre-capillary arterioles. *Microvasc Res.* 2010;
457 80(2):202-8
- 458 15. Kord Valeshabad et al. Conjunctival microvascular haemodynamics in
459 sickle cell retinopathy. *Acta Ophthalmol* 2015; 93(4):275-80
- 460 16. Jiang et al. Functional slit lamp biomicroscopy for imaging bulbar
461 conjunctival microvasculature in contact lens wearers. *Microvascular*
462 *Res.* 2014; 92:62-71
- 463 17. Wang L, Yuan J, Jiang H, Yan W, Cintron-Colon H, Perez V, Cabrera
464 DeBuc D, Feuer W, Wang J. Vessel sampling and blood flow velocity
465 distribution with vessel diameter for characterizing the human bulbar
466 conjunctival microvasculature. *Eye Contact Lens.* 2016; 42(2): 135–
467 140.
- 468 18. To et al. Real-time studies of hypertension using non-mydratic fundus
469 photography and computer-assisted intravital microscopy. *Clin.*
470 *Hemorheol. Microcirc.* 2013; 53(3): 267–279
- 471 19. Khansari et al. Assessment of Conjunctival Microvascular
472 Hemodynamics in Stages of Diabetic Microvasculopathy. *Sci Rep.*
473 2017; 7:45916
- 474 20. Kord Valeshabad A, Wanek J, Mukarram F, Zelkha R, Testai FD,
475 Shahidi M. Feasibility of Assessment of Conjunctival Microvascular

- 476 Hemodynamics in Unilateral Ischemic Stroke. *Microvasc Res.* 2015;
477 100:4–8
- 478 21. Karanam VC, Tamariz L, Batawi H, Wang J, Galor A. Functional slit
479 lamp biomicroscopy metrics correlate with cardiovascular risk. *The*
480 *Ocular Surface.* 2019; 17:64-69
- 481 22. Proesman T, Nuyens D, Vandervoort P, Van Herendael H, Rivero-
482 Ayerza M. First results from a digital mass screening for atrial
483 fibrillation using a smartphone application. *Circulation.* 2018;
484 138(1):A15960
- 485 23. Rajalakshmi R et al. Automated diabetic retinopathy detection in
486 smartphone-based fundus photography using artificial intelligence.
487 *Eye.* 2018; 32:1138-1144
- 488 24. Russo A, Morescalchi F, Costagliola C, Delcassi L, Semeraro F. A
489 novel device to exploit the smartphone camera for fundus photography.
490 *J Ophthalmol.* 2015; 823139
- 491 25. Muiesan ML, Salvetti M, Paini A, Riviera M, Pintossi C, Bertacchini F,
492 Colonetti E, Agabiti-Rosei C, Poli M, Semeraro F, Agabiti-Rosei E,
493 Russo A. Ocular fundus photography with a smartphone device in
494 acute hypertension. *J Hypertens.* 2017; 35:1660–1665
- 495 26. Collings S, Thompson O, Hirst E, Goossens L, George A, Weinkove R.
496 Non-Invasive Detection of Anaemia Using Digital Photographs of the
497 Conjunctiva. *PLoS ONE.* 2016; 11(4): e0153286
- 498 27. Tamir, C. S. Jahan, M. S. Saif, S. U. Zaman, M. M. Islam, A. I. Khan
499 and C. Shahnaz. Detection of anemia from image of the anterior
500 conjunctiva of the eye by image processing and thresholding. *Jn*

Formatted: Font: Italic, Font color: Text 1

- 501 [Humanitarian Technology Conference \(R10-HTC\), 2017 IEEE Region](#)
502 [10, pp. 697-701, 2017.](#)
- 503 28. Otero C, Garcia-Porta N, Tabernerero J, Pardhan S. Comparison of
504 different smartphone cameras to evaluate conjunctival hyperaemia in
505 normal subjects. *Scientific Reports*. 2019; 9(1):1339
- 506 29. [Gottemukkula, V., Saripalle, S., Tankasala, S. P., & Derakhshani, R.](#)
507 [Method for using visible ocular vasculature for mobile biometrics. *JET*](#)
508 [*Biometrics*. 2016; 5\(1\):3-12.](#)
- 509 30. Piepoli et al. 2016 European Guidelines on cardiovascular disease
510 prevention in clinical practice. ESC Guidelines. *European Heart*
511 *Journal*. 2016; 37(29):2315-2381
- 512 31. Forsberg D. Robust image registration for improved clinical efficiency:
513 Using local structure analysis and model-based processing PhD thesis,
514 Linköping University, Medical Informatics, The Institute of Technology,
515 Center for Medical Image Science and Visualisation (CMIV). 2013
- 516 32. Jerman AFT, Pernus F, Likar Z, Spiclin Z. Enhancement of vascular
517 structures in 3D and 2D angiographic images. *IEEE Transactions on*
518 *Medical Imaging*. 2016; 35(9):2108-2118
- 519 33. Duval-Destin M, Murenzi R. "Spatio-Temporal Wavelet: Application to
520 the Analysis of Moving Patterns, in Progress in Wavelets Analysis and
521 Applications. *FrontiReses, Gif-sur-Yvette*. 1993;399-408
- 522 34. Jacques L, Coron A, Vanderghenst P, Rivoldini A. The YAWTb
523 toolbox: Yet another wavelet toolbox. 2001.
524 <https://sites.uclouvain.be/ispgroup/yawtb/doc/YAWTBReferenceManual>
525 [.pdf](#)

Formatted: Font: Not Italic, Font color: Text 1

- 526 35. Koutsiaris AG, Tachmitzi S, Batis N. Wall shear stress quantification in
527 the human conjunctival pre-capillary arterioles in vivo. *Microvascular*
528 *Research*. 2013; 85;34–39
- 529
- 530 36. Pries AR, Secomb TW, Gaehtgens P. Design Principles of Vascular
531 Beds. *Circ Res*. 1995b; 77:1017–1023
- 532 37. Ricci S, Swillens A, Ramalli A, Segers P, Tortoli P. Wall Shear Rate
533 Measurement: Validation of a New Method Through Multiphysics
534 Simulations. *IEEE Trans Ultrason Ferroelectr Freq Control*. 2017;
535 64(1):66-77
- 536